Pharmaceutical Research, Vol. 25, No. 11, November 2008 (© 2008)
DOI: 10.1007/s11095-008-9676-2

Research Paper

Dissolution Improvement and the Mechanism of the Improvement from Cocrystallization of Poorly Water-soluble Compounds

Koji Shiraki,[1,4] Noriyuki Takata,[1] Ryusuke Takano,[1] Yoshiki Hayashi,[2] and Katsuhide Terada[3]

Received April 7, 2008; accepted June 23, 2008; published online July 24, 2008

Purpose. To demonstrate improvement in the dissolution of exemestane and megestrol acetate from cocrystallization using various particle sizes and to investigate the mechanism of the improved dissolution.
Methods. Cocrystal screening was performed by slurry crystallization. The cocrystals were identified and characterized by powder X-ray diffraction, thermal analysis, and single crystal X-ray diffraction. Different particle sizes of each cocrystal were prepared from organic solutions. Solubility and dissolution rates were evaluated using dissolution tests. Transformation behavior of the cocrystals in suspension was analyzed by PXRD and polarization microscopy.
Results. Two novel cocrystals were obtained: exemestane (EX)/maleic acid (MAL) (cocrystal 1) and megestrol acetate (MA)/saccharin (SA) (cocrystal 2). Cocrystal 1 showed a high dissolution rate even with large particles. Cocrystal 2 showed supersaturation with fine particles. The transformation from cocrystal 1 to EX was observed within 1 min in suspension. Cocrystal 2 was transformed to MA within 2–4 h.
Conclusions. Cocrystallizations of EX and MA improved initial dissolution rates compared to the respective original crystals. The mechanism of dissolution enhancement varied. With cocrystal 1, fine particle formation resulted in enhancement, whereas with cocrystal 2, enhancement was due to the maintenance of the cocrystal form and rapid dissolution before transformation to the original crystal.

KEY WORDS: cocrystallization; dissolution; particle size; poorly water-soluble; transformation.

INTRODUCTION

Pharmaceutical cocrystals are crystalline solids containing multiple components, consisting of an active pharmaceutical ingredient (API; host [neutral or in the ionic form]) and a pharmaceutically acceptable compound (guest) (1,2). The hydrogen bond is one of the most important interactions in forming cocrystals. Although cocrystals have long been studied in chemistry, practical usage of cocrystals has only recently emerged in the pharmaceutical industry. Cocrystals are typically found using screening systems and technological advancements in screening have increased the chances of selecting the appropriate cocrystalline active pharmaceutical ingredient (API) form (3).

Cocrystallization improves the physicochemical properties of a drug such as solubility (1,4,5) and stability (6,7). Recently, the number of poorly water-soluble candidates in pharmaceutical drug discovery has increased (8,9). Formulation technologies such as micronization (10,11), nanomization (11–15), solid dispersion (16–18), oil encapsulation (15), and self-emulsified drug delivery systems (15,19,20) improve the bioavailability (BA) of drug candidates with solubility limitations. However, developing a pharmaceutical product using the latest technologies requires time to secure both stability and solubility (21) and selection of a more soluble API form is important. For an ionizable compound, salt formation is a typical strategy because salts show improved solubility by acting as their own buffers to alter the pH of the diffusion layer (22). However, neutral compounds and weak acids or bases often lack the generally needed pK_a difference of three units between acid and base to form a salt crystal (23).

In the case of difficulty in obtaining the appropriate API form, cocrystallization may solve the solubility issue because a significant benefit from cocrystallization of a neutral compound is improved solubility. In addition, the evaluation of the dissolution behavior of a cocrystal and understanding the mechanism are crucial for prediction of absorption and efficient formulation studies. A recent study found that the dissolution profile of the celecoxib/nicotinamide cocrystal depends on the dissolution media or pharmaceutical additives

Electronic supplementary material The online version of this article (doi:10.1007/s11095-008-9676-2) contains supplementary material, which is available to authorized users.

[1] Discovery Platform Technology Department, Chugai Pharmaceutical Co. Ltd., 1-135 Komakado, Gotemba, Shizuoka, 412-8513, Japan.
[2] CMC Planning & Coordination Department, Chugai Pharmaceutical Co. Ltd., 5-5-1 Ukima, Kita-ku, Tokyo, 115-8543, Japan.
[3] Faculty of Pharmaceutical Science, Toho University, 2-2-1 Miyama, Funabashi, Chiba, 274-8510, Japan.
[4] To whom correspondence should be addressed. (e-mail: shirakikj@chugai-pharm.co.jp)

(24). This report highlighted the importance of exploring the conversion of the form of the cocrystal in aqueous media prior to pharmacokinetic studies. The dissolution of the cocrystal of an ionizable drug, the indomethacin/saccharin cocrystal, was influenced by buffer strength in the aqueous medium (2). These reports are among the few related to the dissolution mechanism of cocrystals in aqueous medium and more study is required to reveal the full potential of cocrystals. Particle size is generally an important and controllable parameter of API forms, including cocrystals, and influences dissolution behavior and absorption. Little is known about the effect of the particle size on the dissolution and transformation behavior of a cocrystal.

The major objectives of the present study are the following. (1) Identify new cocrystals from neutral compounds. (2) Demonstrate the differences between the dissolution behavior of the newfound cocrystal and its host crystal. (3) Demonstrate the effect of particle size on the dissolution behavior of the new cocrystal. (4) Investigate the relationship between the dissolution behavior and the solid state. Exemestane (EX), 6-methylenandrosta-1,4-diene-3,17-dione, and megestrol acetate (MA), 17 alpha-acetoxy-6-methylpregna-4,6-diene-3,20-dione, both poorly soluble and neutral drugs, were selected to be the model compounds for this study. Each crystal structure was reported previously (CSD refcodes PEKFAN [EX] and KUHZAO [MA]). EX, a steroidal aromatase inhibitor, decreases contralateral new breast cancer in postmenopausal women when taken in the adjuvant setting (25) and is categorized as BCS Class II. MA reduces the suffering caused by advanced breast and endometrial cancers and treats loss of appetite and severe weight loss in patients with acquired immunodeficiency syndrome (AIDS) (26,27). MA requires micronization or nanomization to improve BA (28).

In order to find cocrystals of the model compounds, we conducted cocrystal screening with various guests. The two carbonyl groups in EX and three carbonyl groups in MA have the potential of hydrogen bonding. We selected guests that had the functional groups (–OH and/or –NH). From thermal analysis, powder X-ray diffraction (PXRD), and single crystal X-ray diffraction, two novel cocrystals were identified and characterized: EX with maleic acid (MAL) (cocrystal 1) and MA with saccharin (SA) (cocrystal 2). Fig. 1 shows the chemical structure of each component. We prepared various sizes of particles of the two cocrystals and, using a dissolution test system, evaluated dissolution improvement by comparing the cocrystals with the original compounds. To reveal the mechanisms of dissolution improvement from cocrystallization, transformation behavior of each cocrystal in an aqueous suspension was analyzed by PXRD and observed using polarization microscopy.

MATERIALS AND METHODS

Materials

EX was isolated from Aromasin® tablets (Pfizer Japan Inc., Tokyo, Japan). MA was purchased from Sigma-Aldrich (St. Louis, MO, USA). The guest compounds and crystallization solvents used in this study are listed in Tables I and II, respectively. The chemicals were purchased from various commercial suppliers.

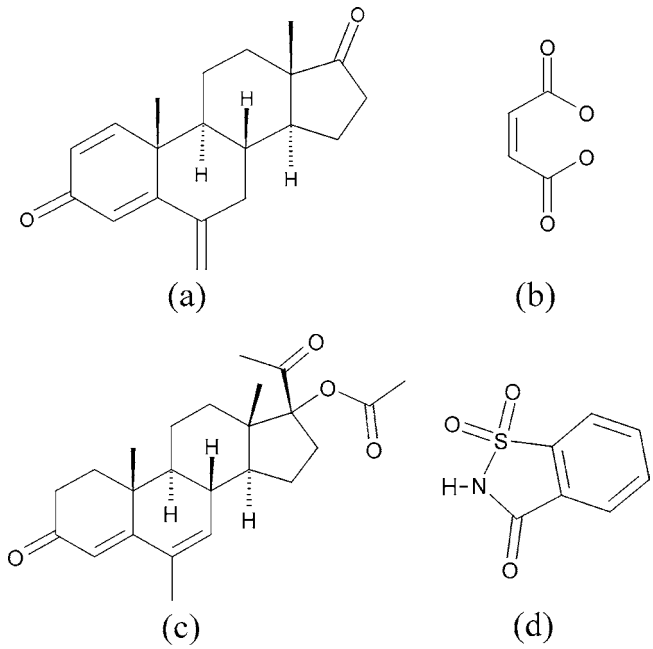

Fig. 1. Chemical structures of host and guest compounds; **a** EX, **b** MAL, **c** MA, **d** SA.

Cocrystal Screening

Cocrystal screening of the two host compounds was conducted with 14 guest compounds for EX and 15 guest compounds for MA (Table I). The screening was conducted using the slurry method (29) as previously reported (30). A total of 29 combinations of host and a guest were each dissolved in dimethyl sulfoxide (DMSO) at a 1:1 molar ratio (200 mg/mL). Each DMSO solution containing a host and a guest mixture (4 mg) was dispensed to a 0.6-mL glass vial with a screw cap and polytetrafluoroethylene-coated rubber septum. Each was then lyophilized at −20°C. Cocrystallization

Table I. Guest Compounds

Model compounds	
Exemestane	Megestrol acetate
Adipic acid	Adipic acid
Benzenesulfonic acid	Benzenesulfonic acid
Benzoic acid	Benzoic acid
Citric acid	Citric acid
Fumaric acid	Fumaric acid
L-Lactic acid	L-Lactic acid
Maleic acid	Maleic acid
Malonic acid	–
L-Malic acid	L-Malic acid
Salicylic acid	Salicylic acid
–	Succinic acid
L-Tartaric acid	L-Tartaric acid
D-Tartaric acid	D-Tartaric acid
Meso-tartaric acid	–
–	Saccharin
Nicotinamide	Nicotinamide
–	Urea

Endash (–) Test not conducted

Table II. Crystallization Solvents and Forms Obtained from Screening

Solvents	Cocrystal 1	Cocrystal 2
Ethanol	Host	Cocrystal
2-Propanol	Host	Cocrystal
1-Hexanol	Host	Cocrystal
Acetonitrile	Host	Cocrystal
Ethyl acetate	Cocrystal	Cocrystal
1-Propyl acetate	Cocrystal	Cocrystal
Hexyl acetate	Host	Cocrystal
N,N-dimethylformamide (DMF)	Host	nc
DMF/diisopropyl ether=1/3 (*v*/*v*)	nc	Cocrystal
Acetone	*n*	Cocrystal
Methyl ethyl ketone	*n*	Cocrystal
Methyl propyl ketone	Cocrystal	Cocrystal
Diisopropyl ether	nc	Cocrystal
Tetrahydrofuran (THF)	*n*	nc
THF/heptane=1/3 (*v*/*v*)	nc	Cocrystal
Toluene	Cocrystal	Cocrystal
Dichloromethane	Cocrystal	Cocrystal
Distilled water	Host	Cocrystal

n Solution or small amount of sample, *nc* test not conducted

was performed using the solvents listed in Table II. Each crystallization solvent was dispensed to a vial (20 μL/vial to attain homogeneity) and the slurries were stored for 8 days at ambient temperature with slow shaking at 100 rpm using a Taitec NR-30 rotary shaker. The solids in the vials were collected and fixed onto circular stainless steel meshes (in-house, 4 mm in diameter) using Pasteur pipettes and micro-spatulas for powder X-ray diffraction (PXRD) analysis and subsequently sorted into groups of unique PXRD patterns. The samples selected from each group were subjected to thermogravimetric/differential thermal analysis (TG/DTA).

Sample Preparation

EX Isolation and Crystallization

Aromasin® tablets containing 25 mg exemestane (130 tablets) were milled using a mortar and then dissolved in ethyl acetate (500 mL). The solution was filtrated and the contaminants extracted from the formulation by liquid–liquid extraction twice using distilled water. The ethyl acetate phase was retrieved and evaporated. The residual solid was suspended twice using distilled water (100 mL). The second suspension was filtrated and the residual solid was dissolved by ethyl acetate. Na_2SO_4 was added to the solution to remove residual water, the solution filtrated and evaporated to yield the residual solid, EX, (3.04 g). EX was dissolved in ethyl acetate (50 mL) and hexane (100 mL) added at 40°C. The solution was cooled for more than 8 h to 5°C. The EX crystals were generated in the solution and isolated by filtration, then dried in vacuo at 25°C (1.31 g), sieved (106-, 150-, 300-μm mesh openings), and recovered from the 106-μm and 150-μm mesh sieves. Purity was determined by elemental analysis (calculated: C, 81.04%; H, 8.16%; O, 10.80%; observed: C, 80.97%; H, 8.17%; O, 10.88%). In order to obtain finer EX particles, crystallized EX (200 mg) was dissolved in ethyl acetate (2 mL) at 80°C, cooled to 40°C, and hexane (4 mL) added. The solution was cooled to 25°C and sonicated for 1 min. The EX crystals were rapidly generated in the solution, isolated by filtration, and dried in vacuo at 25°C (147 mg). Particle size averaged about 9 μm in diameter. Purity was determined by elemental analysis (observed: C, 81.01%; H, 8.17%; O, 10.89%).

EX/MAL Cocrystal (cocrystal 1)

Crystallized EX (800 mg) and MAL (313 mg) were dissolved in methyl ethyl ketone (8 mL) at 80°C in a sealed glass vial and cooled to 25°C. Heptane (20 mL) was added and the solution cooled to 5°C. Cocrystal 1 was gradually generated from the solution and then isolated by filtration and dried in vacuo at 25°C (760 mg). Crystalline Cocrystal 1 was sieved (106-, 150-, and 300-μm mesh openings) and recovered from the 106 and 150-μm mesh sieves. In order to obtain finer particles of cocrystal 1, crystallized EX (800 mg) and MAL (313 mg) were dissolved in methyl ethyl ketone (2 mL) at 80°C, cooled to room temperature, heptane (4 mL) added, and sonicated for 3 min. Cocrystal 1 was rapidly generated in the solution, isolated by filtration, and then dried in vacuo at 25°C (835 mg). Particle size averaged about 10 μm in diameter.

MA

MA was used as purchased. Particle size averaged about 15 μm.

MA/SA cocrystal (cocrystal 2)

MA (400 mg) and SA (222 mg) were dissolved in acetone (9 mL) at 80°C, cooled to 25°C, and shaken for 2 days. Cocrystal 2 was gradually generated from the solution and filtrated and dried by vacuum dryer at 25°C (292 mg). Cocrystal 2 was sieved (106-, 150-, and 300-μm mesh openings) and recovered from the 106-μm and 150-μm mesh sieves. In order to obtain finer particles of cocrystal 2, MA (200 mg) and SA (111 mg) were dissolved in acetone (3 mL) at 85°C, cooled, and sonicated for 3 min at room temperature. The cocrystal was rapidly generated in the solution and isolated by filtration and then dried in vacuo at 25°C (190 mg). Particle size averaged about 15 μm.

Solid Analysis

Powder X-ray Diffraction (PXRD)

PXRD measurements of all samples were conducted in reflectance mode using a Bruker D8 Discover with a GADDS CS diffractometer (Bruker AXS GMBH, Karlsruhe, Germany) using Cu Kα radiation with a graphite monochromator and a 0.3-mm single pinhole collimator. The tube voltage and amperage were set respectively to 45 kV and 40 mA. The diffractometer was equipped with an XYZ sample stage and a Hi-STAR area detector located 25 cm (2θ=5–25°) from the sample. The acquisition time was 90 s per frame.

The PXRD patterns in the range of 3° to 35° 2θ were obtained using a Spectris X'Part PRO MPD diffractometer (PANalytical Japan spectris Co. LTD., Tokyo) using Cu Kα

radiation in reflectance mode. Tube voltage and amperage were set at 50 kV and 40 mA, respectively. Divergence and scattering slits were set at 0.25°, and the receiving slit was set at 0.1 mm. The samples were packed in an aluminum sample holder and measured by a continuous scan at 3°/min with a step size of 0.02° 2θ.

Thermal Analysis

TG/DTA of the screening samples was performed using an EXSTAR6200 TG/DTA system (SII NanoTechnology Inc., Tokyo, Japan). All measurements were carried out in open aluminum pans, heated from 30°C to 350°C at a heating rate of 10°C/min under a nitrogen purge. All samples other than screening samples were accurately weighted (1–3 mg) and analyzed in the same manner as the screening samples.

Differential scanning calorimetry (DSC) of all samples other than the screening samples was conducted using an EXSTAR6200R DSC system (SII NanoTechnology Inc.). All measurements were conducted in sealed non-hermetic aluminum pans. The samples were heated at a rate of 10°C/min under a nitrogen purge. Typical samples were accurately weighted (2–5 mg).

Host/Guest Composition Analysis

The molar ratio for each size of cocrystal was determined by 1H NMR (DMSO-*d*6) spectroscopy (JEOL JNM-ECP 400 MHz, JEOL Ltd., Tokyo, Japan).

Particle Size Analysis

Particle images of the finer particles (more than 1,000) were taken using digital microscopes VH-Z450 and VH-8000 (Keyence Co., Osaka, Japan) and analyzed using Image-pro® PLUS 5.12 (Media Cybernetics Inc., MD, USA). The Feret's diameter was measured and the number mean size was calculated.

Single Crystal X-ray Diffraction

Single crystals were isolated from the prepared cocrystals. Data were collected using an AFC7R four-circle diffractometer (Rigaku Co., Tokyo, Japan) with a graphite monochromated Cu Kα radiation source at 298 K. Three standard reflections were measured every 150 reflections. 2θ–ω scans were employed for data collection, and Lorentz and polarization corrections were applied. The structures were solved by a direct method using SIR92 (31) and refined using CrystalStructure ver.1.10 (Rigaku). All H atoms of MA and SA were placed on the difference map and were constrained during the refinement. Methyl H and methylidene H of EX and hydroxyl H of MAL were placed on the difference map and were constrained during the refinement. Other H atoms of EX and MAL attached to carbon were positioned geometrically and refined as riding. Additional details of data collection and structure refinement are given in Table III.

Table III. Crystallographic Data for Cocrystal 1 and Cocrystal 2

Compound	Cocrystal 1	Cocrystal 2
Empirical formula	C24H28O6	C31H37NO7S
Formula weight	412.8	567.7
Temperature (K)	298.1	298.1
Crystal size (mm)	0.40×0.18×0.14	0.40×0.10×0.10
Crystal system	Monoclinic	Orthorhombic
Space group	P21	P 21 21 21
a (Å)	10.8714(8)	16.0425(14)
b (Å)	17.4034(12)	25.475(2)
c (Å)	5.8498(5)	6.9358(10)
α (°)	90.0000	90.0000
β (°)	100.541(6)	90.0000
γ (°)	90.0000	90.0000
Volume (Å^3)	1,088.10(14)	2,834.5(5)
Z	2	4
ρ_{calc} (g cm^{-3})	1.259	1.330
No. of reflections collected	3,220	5,575
No. of unique reflections	2,336	3,647
No. of parameters	300	399
R1 [$I>2\sigma(I)$]	0.0617	0.0342
wR2 (all data)	0.1435	0.1087
Goodness-of-fit on F2	1.097	0.963

Intrinsic Dissolution Test and Dissolution Test for Powder

Measurements for the tests were taken as described previously (32). In brief, the dissolution tests were conducted using a VK7010 dissolution station and a VK8000 dissolution sampling station with a 100-mL conversion kit (Vankel Technologies, Inc., NC, USA) and were carried out for 30 min or 4 h in 50 mL of fasted-state simulated fluid (FaSSIF) at 37°C with a paddle speed of 50 rpm.

For the intrinsic dissolution test, about 5 mg of each of the fine samples (EX, cocrystal 1, MA, and cocrystal 2) was compressed into a 0.071 cm^2 disk by a hydraulic press at ~100 MPa for 1 min using a die with a hole 0.3 cm in diameter (Spectra-Tech, Inc., CT, USA). The disk was compressed to provide a flat surface on one side of the die; the other side of the die was sealed. The dissolution studies lasted 4 h, after which time the disks were recovered and quickly checked by PXRD for presence of a cocrystal. For EX, MA, and cocrystal 1, the initial dissolution rate was calculated using the data from 5–30 min. For cocrystal 2, data from 5–15 min was used because the dissolution rate gradually slowed. Experiments were run in triplicate.

All fine samples were agglomerated and all samples showed low wettability with significant difference. Therefore, agglomeration and wettability were improved in order to investigate the potential dissolution improvement of each particle size. Hence, samples for the powder dissolution tests were prepared from a physical mixture of drug and α-lactose (1/10; *w*/*w*). The sample amount of EX and cocrystal 1 applied was approximately 1 mg or 20 mg, and that of MA and cocrystal 2 was approximately 2 mg. The amount of cocrystal was converted to that of the host compound. The dissolution studies lasted 30 min or 4 h. Experiments were run in quadruplicate.

Drug concentrations were determined by high performance liquid chromatography (HPLC; Waters 2795 separation module, Waters, Milford, MA) using a UV detector (Waters 2487 dual λ UV/VIS detector, Waters) and a C18 column (Catenza CD-C18 3 μm 3.0×50 mm, Imtakt Corporation, Kyoto, Japan). The wave length for EX and MA was set at 245 and 288 nm, respectively.

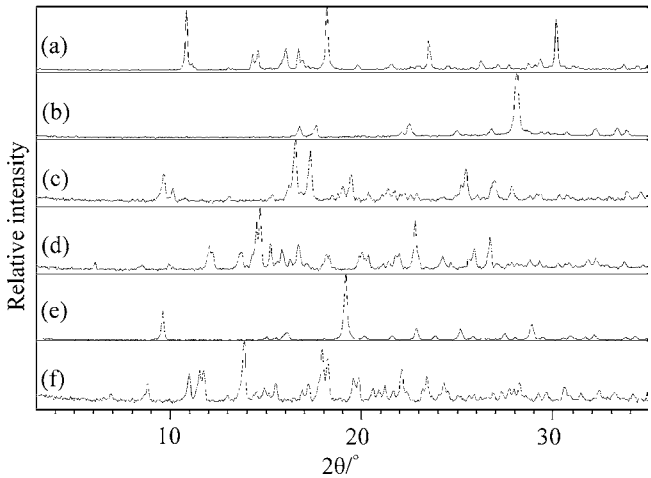

Fig. 2. PXRD pattern of *a* EX, *b* MAL, *c* cocrystal 1, *d* MA, *e* SA, *f* cocrystal 2.

Transformation Behavior

PXRD Analysis

Cocrystals (~1 mg) of all sizes were suspended in FaSSIF (1 mL for cocrystal 1 and 10 mL for cocrystal 2) at 37°C. The precipitates with different suspension times were collected, then quickly filtrated and analyzed by PXRD. Sampling was conducted until the cocrystal had transformed to the host compound form. Experiments were run in triplicate for each particle size.

Observation of Transformation

After adding FaSSIF to the fine and 150–300-μm range cocrystals, dissolution and transformation was observed on glass slides using polarization microscope model OPTIPHOT-PDL (Nikon Co., Tokyo, Japan). The concentration in the suspension was adjusted to ~1 mg/mL for cocrystal 1 and to ~0.1 mg/mL for cocrystal 2. The particle size of cocrystal 1 after adding FaSSIF was measured using the same polarization microscope and Image-pro® PLUS (Media Cybernetics).

RESULTS AND DISCUSSION

Cocrystal Screening and Solid Analysis

The formations of cocrystals were indicated from the screening of the combination of EX with MAL and MA with SA. Unique PXRD patterns and TG/DTA curves distinguishable from the host and the guest were observed. The TG/DTA curves of the unique crystals suggested they were nonsolvate crystals. The forms obtained from the various crystallization solvents used are listed in Table II. The solvents that resulted in a novel crystal in the screening of EX/MAL were ethyl acetate, 1-propyl acetate, methyl propyl ketone, toluene, and dichloromethane. A novel crystal of MA/SA was found with all solvents used.

The ratio of host/guest (EX/MAL and MA/SA) in the novel crystals for each particle size was determined by 1H NMR and found to be 1 to 1, regardless of particle size. All sized particles showed the same PXRD pattern and TG/DTA

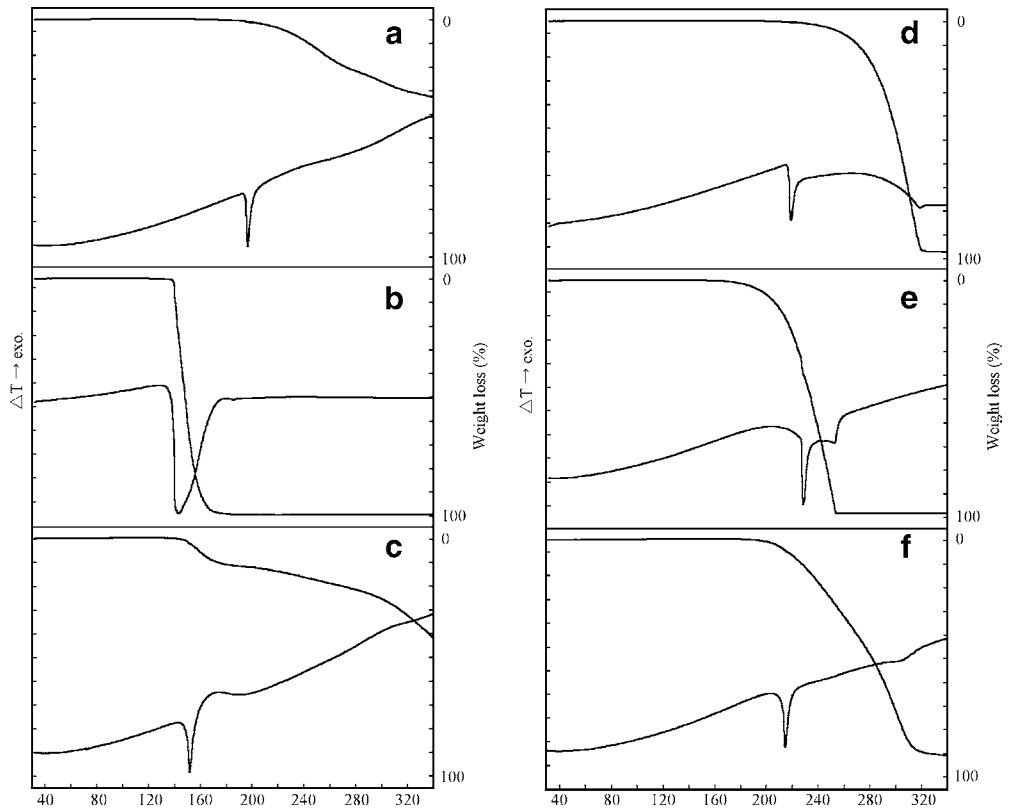

Fig. 3. TG/DTA chart of **a** EX, **b** MAL, **c** cocrystal 1, **d** MA, **e** SA, **f** cocrystal 2.

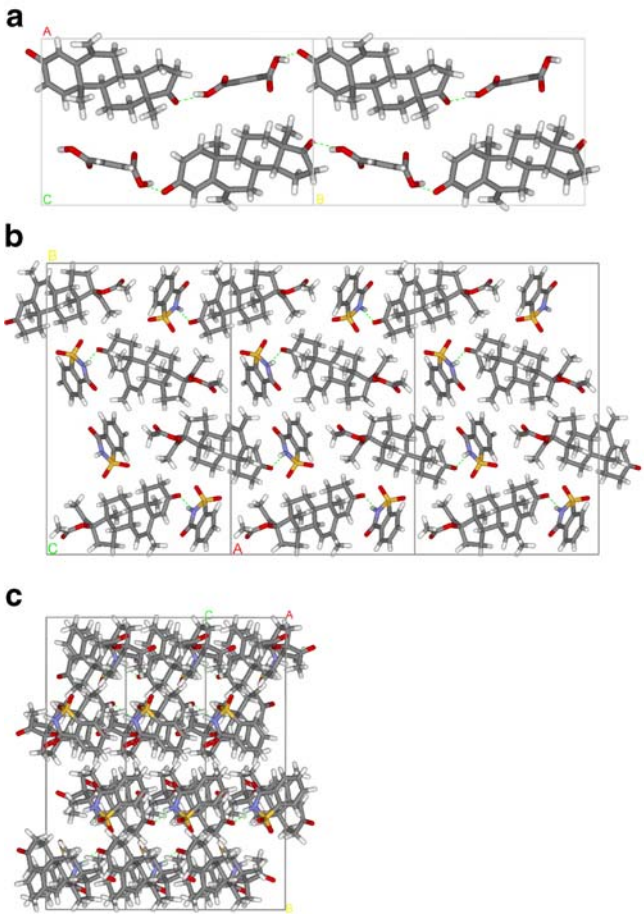

Fig. 4. Packing diagram along the *ab* plane for **a** cocrystal 1, the *ab* plane for **b** cocrystal 2, and the bc plane for **c** cocrystal 2.

curve as the new forms obtained from screening. From the TG/DTA data, no residual solvents from any sized sample were detected and all sized samples were determined to be cocrystals (EX/MAL [cocrystal] 1 and MA/SA [cocrystal 2]). Examples of the PXRD patterns (Fig. 2) and TG/DTA curves (Fig. 3) from each host, guest, and cocrystal are given. From DSC analysis, the melting point of each cocrystal (~147°C for cocrystal 1 and ~214°C for cocrystal 2) was found to be different from that of their respective host and guest compounds.

Cocrystal 2 was found with all solvents used, suggesting that the interaction between MA and SA may be stronger than the interaction between any of the crystallization solvents and MA or SA. Previous research indicates that the phase solubility diagrams of cocrystals are affected by the concentration of each component in solution and the amount of solution complexation that occurs (33). Therefore, it is important to use various solvents in the slurry crystallization of cocrystal screening.

Thermal analysis confirmed that both MAL and SA lost weight after melting, suggesting decomposition, and the boiling of MAL, and/or conversion of MAL into fumaric acid, as reported in the literature (34–37). Since MAL and SA rapidly decomposed after the crystal melted, cocrystal preparation using a melting method as previously reported (38) would be difficult. The exothermic behavior after the melting of cocrystal 1 was considered to be from the chemical reaction of the EX and MAL and/or transformation to EX or transformation of another cocrystal. Further study is needed to clarify the exothermic behavior.

The crystal structure of each cocrystal was confirmed by single crystal X-ray diffraction analysis. The crystallographic data of the cocrystals is summarized in Table III and the crystal structures are shown in Fig. 4. In cocrystal 1, two carboxylic acid groups of MAL formed hydrogen bonds with the carbonyl groups on the C(3) and C(17) positions of EX and a head-to-tail chain structure is formed. The molar ratio of host and guest compound for cocrystal 1 was 1 to 1 (Fig. 4a). In cocrystal 2, the NH of the *N*-acyl sulfonamide groups of the SA formed hydrogen bonds to the carbonyl groups on the C(3) position of MA. The molar ratio of host and guest compound for cocrystal 2 was 1 to 1 (Fig. 4b,c). The simulated PXRD patterns from the single crystal X-ray diffraction data matched the experimental PXRD patterns.

From a search using ConQuest V.1.1 (Cambridge Crystallographic Data Center, Cambridge, UK), no examples of these cocrystals were found in the Cambridge Structural Database (CSD version 5.29).

Dissolution Test

Intrinsic dissolution tests were conducted to compare the dissolution rate of a cocrystal and with its host crystal. Table IV shows the intrinsic dissolution rates for each sample. Cocrystal 1 showed the same dissolution rate as EX. The dissolution rate for cocrystal 2 was three to four times higher than MA, but there was a wide variation in the dissolution.

The residual solid from cocrystal 1 transformed to the host crystal (Fig. 5a). Residual cocrystal 2 had mostly maintained its cocrystal form but did contain a small amount of host crystal (Fig. 5b). Because cocrystals transform to host crystals, accurate evaluations are difficult (39). However, the initial dissolution rate of MA was improved by cocrystallization with SA.

To examine the supersaturation of each cocrystal in comparison with each host compound powder dissolution tests applying ~20 mg for EX and cocrystal 1 (EX concentration 0.4 mg/mL) and ~2 mg for MA and cocrystal 2 (MA concentration 0.04 mg/mL) were conducted. The concentrations of the solid were about 10-fold the saturated solubility of the host compounds (non-sink condition).

None of the dissolution profiles for cocrystal 1 showed supersaturation. The maximum concentration of cocrystal 1

Table IV. Intrinsic Dissolution Rate of EX, Cocrystal 1, MA, and Cocrystal 2 in FaSSIF at 37°C

EX ($\mu g\ cm^{-2}\ min^{-1}$)	Cocrystal 1 ($\mu g\ cm^{-2}\ min^{-1}$)	MA ($\mu g\ cm^{-2}\ min^{-1}$)	Cocrystal 2 ($\mu g\ cm^{-2}\ min^{-1}$)
3.81±0.46	4.19±1.17	0.66±0.03	2.53±0.91[a]

[a] Intrinsic dissolution rate was calculated from 5–15 min data.

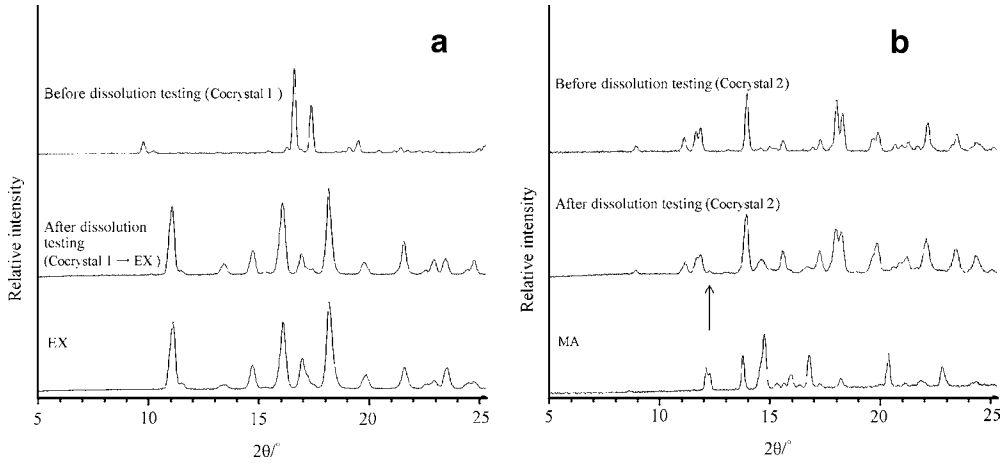

Fig. 5. PXRD pattern changes in the residual solid from the intrinsic dissolution test; **a** cocrystal 1, **b** cocrystal 2, the *arrow* shows the peak of MA.

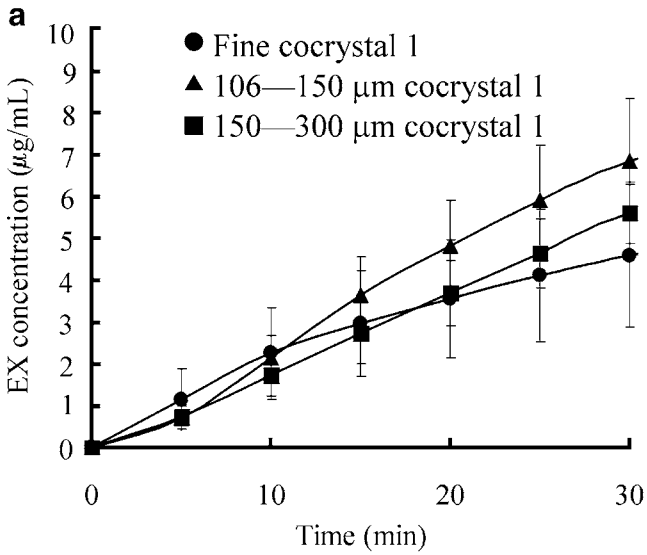

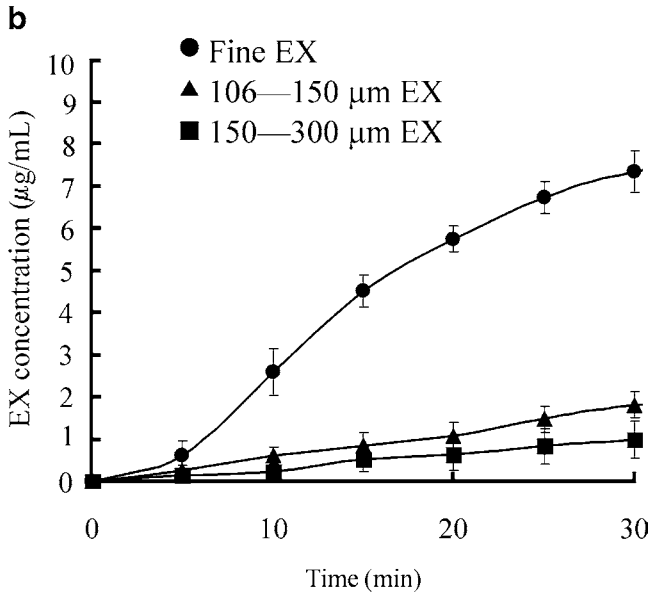

Fig. 6. Dissolution profiles of cocrystal 1 and EX in FaSSIF (*error bars* show SD, $n=4$): **a** cocrystal 1, **b** EX.

and EX was ~0.05 mg/ml (saturated solubility of EX), similar to the dissolution profiles. To determine the dissolution rate of EX and cocrystal 1 for the various particle sizes, the amount of test sample was decreased to 1 mg (sink condition). Fig. 6a shows the dissolution rate of cocrystal 1. Particle size did not significantly affect the dissolution rate of cocrystal 1. For comparison, a dissolution test of EX was conducted (Fig. 6b). The smaller particle sizes dissolved at a higher rate (fine > 106–150 μm > 150–300 μm) as described by the Noyes–Whitney equation (40). The dissolution rates for all sizes of cocrystal 1 were close to that of the fine EX but the variability of the dissolution of cocrystal 1 was greater than that of EX. We concluded that dissolution was influenced by the transformation of cocrystal 1 to host crystal and/or by changes in the state of the transformed particle such as reduced size or agglomeration.

On the other hand, the dissolution profile of fine cocrystal 2 showed supersaturation (Fig. 7). The supersaturated concentration of MA from cocrystal 2 at 15 min was about six times greater than the saturated concentration of

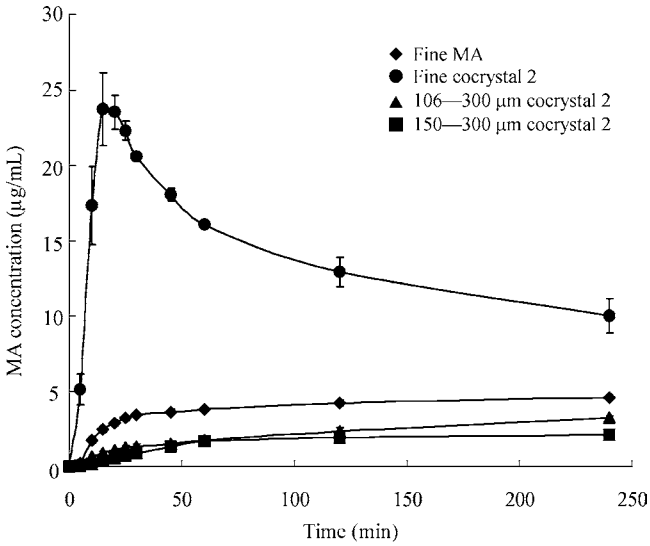

Fig. 7. Dissolution profiles of MA and cocrystal 2 in FaSSIF (*error bars* show SD, $n=4$).

the fine MA (~4 μg/mL), and within 4 h, was two times greater. Cocrystal 2 in the ranges of 106–150 and 150–300 μm particle size did not show supersaturation. Particle size reduction of cocrystal 2 significantly affected both the supersaturation and the dissolution rate and the dissolution was significantly improved by cocrystallization compared to fine MA. Although cocrystal 2 also apparently converted to MA crystals in the media, it was assumed that the temporal supersaturation was caused by the short time cocrystal 2 maintained its form. Larger-sized cocrystal 2 was assumed to transform to MA before showing supersaturated concentration because of the slower dissolution rate of large particles.

The solubility of EX and MA in FaSSIF was improved by cocrystallization. Improvement of the dissolution profile by cocrystallization has been reported in various media, for example, in 0.1 N HCl at 25°C for a cocrystal of itraconazole, a week acid (4), and in pure water for a cocrystal with fluoxetine hydrochloride, a salt (1). The effect of gastric conditions including pH is another important consideration. Therefore, validation from *in vivo* absorption studies is needed. However, dissolution in a physiologically-based medium such as FaSSIF is beneficial in determining the dissolution profile of a drug and is relevant to *in vivo* behavior (32).

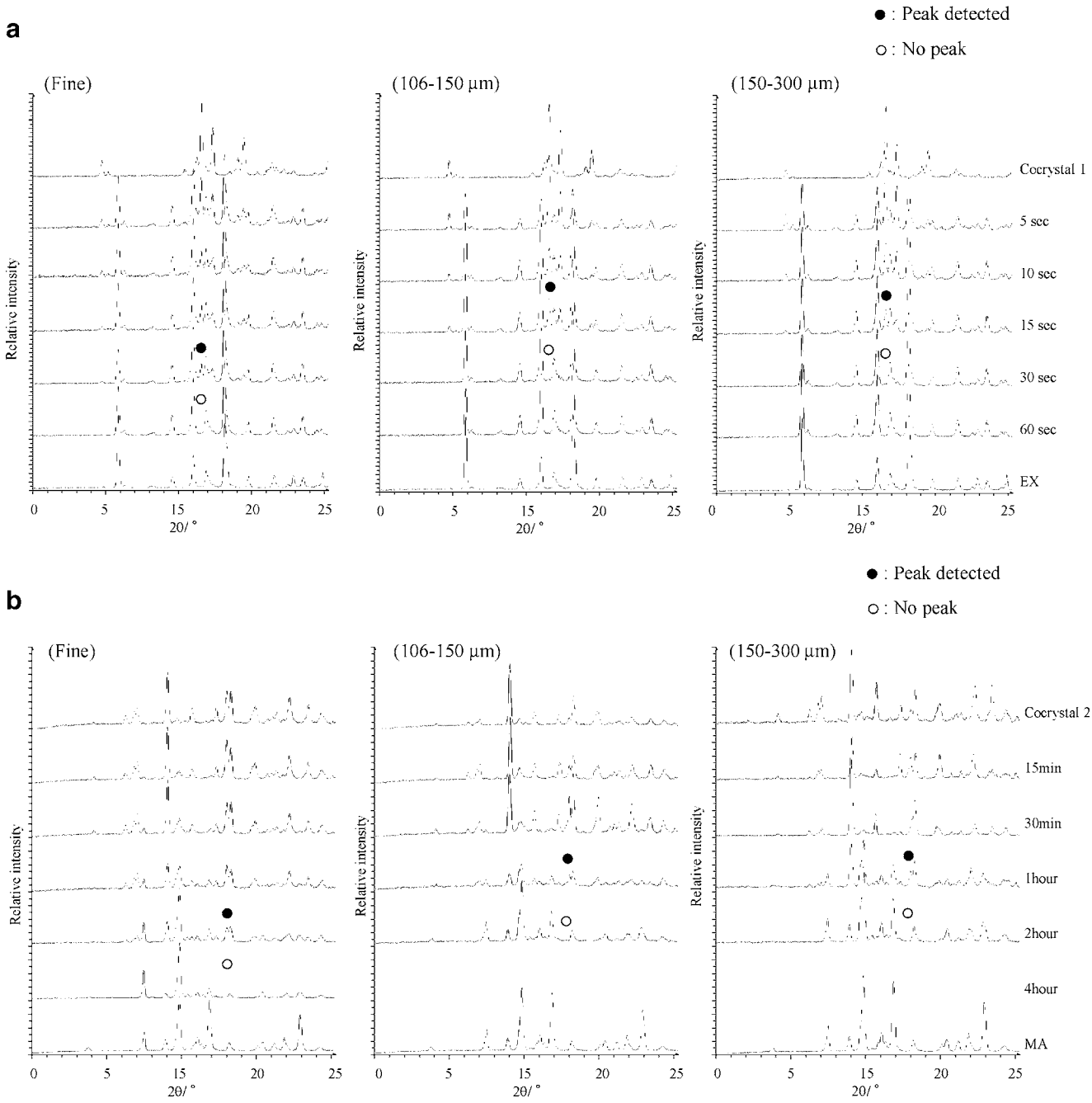

Fig. 8. PXRD pattern changes for **a** cocrystal 1 and **b** cocrystal 2 at different suspending time.

Cocrystals have shown the potential to improve absorption. For example, within the same size range samples, such as with the 150–300 μm range of EX and of cocrystal 1 administered in animal models, there is the possibility of better absorption of the cocrystal. In the case of dosing fine EX, the absorption will be almost the same as any particle size of cocrystal 1 and thus the particle size of EX will need to be rigidly controlled by milling or crystallization. Although cocrystal 2 in the ranges of 106–150 and 150–300 μm may not improve absorption, fine cocrystal 2 exhibited supersaturated concentration in this study and so shows potential absorption improvement. Even if the supersaturation is tentative, the solubility will have an impact on absorption (41). However, particle size reduction will be needed to increase the supersaturation and enhance absorption. For improvement of absorption of MA, the particle size needs to be reduced to several hundred nanometers using technology such as Nano-Crystal® (28). Even with the necessity of controlling particle size (~15 μm), cocrystal selection is valuable.

Further improvement of the dissolution of cocrystals 1 and 2 may be possible through formulation studies applying technologies such as micronization and selection of additives. If solubility can be improved in a general formulation study, cocrystallization might be advantageous and reduce the effort

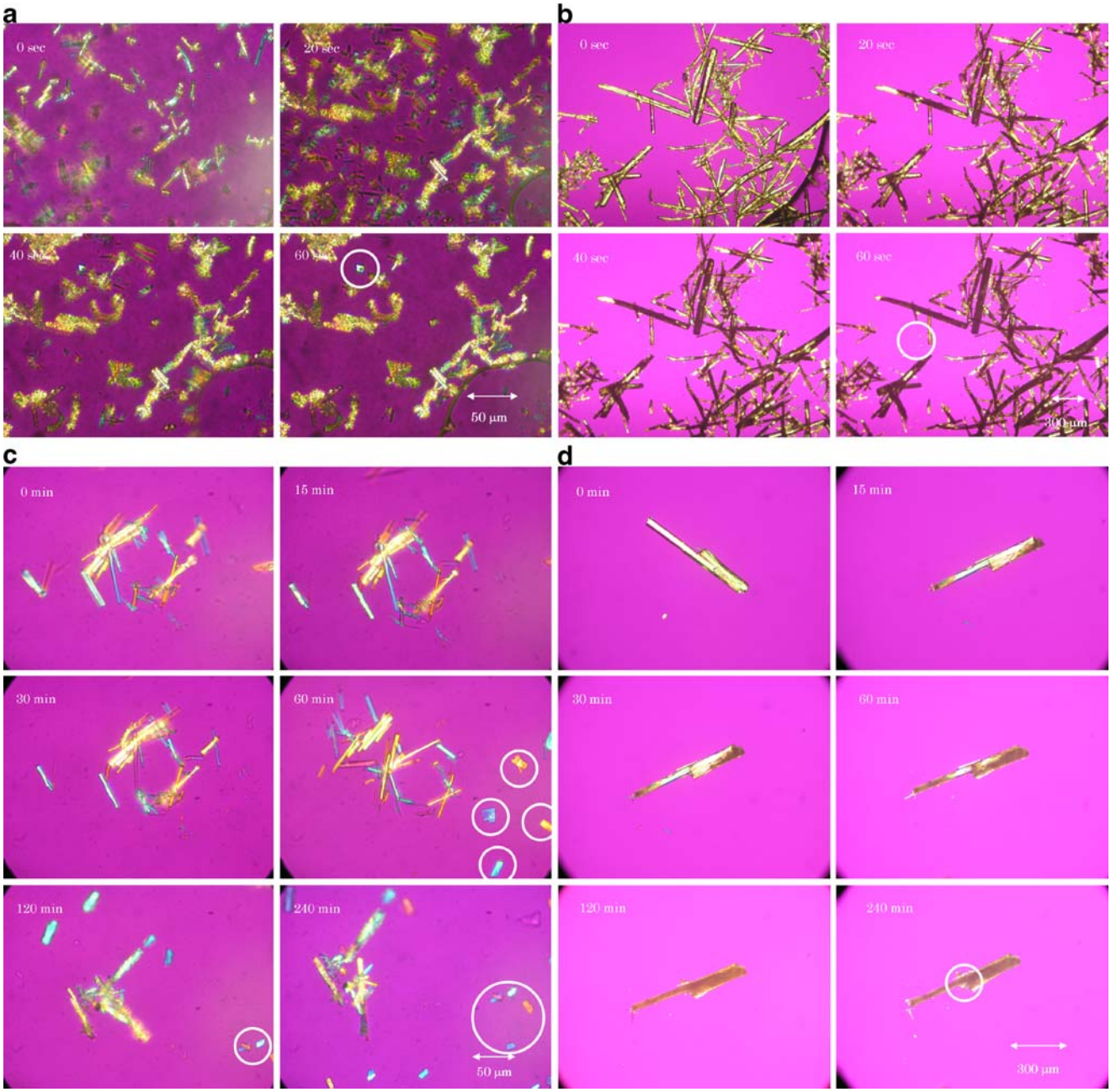

Fig. 9. Observation of transformation behavior in FaSSIF suspensions; **a** fine cocrystal 1, the *circle* shows slight crystal growth, **b** 150–300 μm cocrystal 1, the *circle* shows formed small particles, **c** fine cocrystal 2, the *circles* show precipitated particles, and **d** 150–300 μm cocrystal 2, the *circle* shows formed small particles.

and/or time required for the study. The dissolution behavior of the celecoxib/nicotinamide cocrystal has shown improvement by additives (24).

Transformation Behavior

The time-dependent change in the form and state of the cocrystals were evaluated from PXRD analysis and polarization microscopy. Fig. 8 shows examples of the results of PXRD. Changes in the time-dependent patterns demonstrate transformation from cocrystal to host crystal. Cocrystal 1 transformed to EX within 1 min (Fig. 8a). Although the effect of particle size on transformation rate for cocrystal 1 is difficult to analyze quantitatively due to rapid transformation and the preferred orientation of the crystals, the transformation rate of fine cocrystal 1 was relatively slower than for the larger-sized particles (106–150 and 150–300 μm). In contrast, cocrystal 2 gradually transformed to MA and had completely transformed to MA in 2–4 h (Fig. 8b). The transformation time of the fine cocrystal 2 was about 2 h slower than the larger-sized cocrystal 2.

Observation of both cocrystals under polarization microscopy revealed that transformation occurred from more than one point and then expanded to the whole crystal (Fig. 9). The transformation rate as well as PXRD results for cocrystal 1 was faster than for cocrystal 2. During the transformation of fine cocrystals, precipitation and slight crystal growth were observed (Fig. 9a, c). Large-sized cocrystals (150–300 μm) transformed to the host crystals, maintained the shape temporarily, and then the transformed particles dissociated and smaller particles were generated (Fig. 9b, d).

The transformation rate for the fine particles of both cocrystals was slower than for the larger-sized particles. We suggest three major reasons. (1) The larger specific surface area of fine particles requires more time for transformation from cocrystal to host crystal, based on the assumption that fine and large cocrystals have the same surface state (*i.e.* morphology, disorder of the crystal surface *etc.*). (2) The ratio of major to minor crystal surface area is different between fine and large particles. The large cocrystals mainly consisted of a surface in which guest molecules easily dissociated from the cocrystal. (3) The concentration of guest inside the agglomeration of fine cocrystal increases during cocrystal transformation and guest molecules dissociate. When fine cocrystals are partly dissolved and the concentration of guest compound increases inside the agglomerate, there is the possibility that, without agitation, a slower transformation will occur. There was no transformation from cocrystal 1 to the host compound found in the high-concentration MAL solution within the first 8 h. For example, carbamazepine/nicotinamide cocrystal can be prepared in water by suspending carbamazepine in a saturated solution of nicotinamide (42).

The transformation rate of cocrystal 1 was faster than that of cocrystal 2. It has been suggested that the solubility of cocrystals with the same host compound is influenced by guest compound solubility and that the order of solubility of the guest compounds correlates with the cocrystal intrinsic dissolution rate (1). It is presumed that the thermodynamic factor between host and guest compounds is also important for cocrystal solubility (5). In the present study, cocrystal 1 and cocrystal 2 have different host compounds so they cannot be compared with respect to thermodynamics or crystal structure. However, the higher solubility of MAL (440 mg/mL at 25°C) (43) compared with SA (4.3 mg/mL at 25°C) (43) may have effected the higher transformation rate of cocrystal 1 compared with cocrystal 2.

Relationship Between Dissolution and Transformation Behavior

The transformation mechanism of the cocrystals is considered to be solution-mediated and includes dissociation of the guest compounds. Changes in the dissolution behavior of the particles as a result of transformation are important for absorption. In this study, we found it crucial that small particles were generated and particle shape maintained after and/or during transformation. We think that the variability in the dissolution profile of cocrystal 1 was a result of the complex process of crystal growth and/or small particle generation after transformation.

The mean particle size of the EX generated from cocrystal 1 of size 150–300 μm in suspension was ~4 μm, with particle size distribution the same as for the original fine EX in suspension (Fig. 10), again showing that the dissolution profile of cocrystal 1 is similar to fine EX. Dissolution of smaller particles is generally faster than with larger particles but the dissolution rates for the various sizes of cocrystal 1 did not follow this principle. We concluded that the transformation rate from cocrystal 1 to EX was rapid, and with the finely powdered form, the transformed EX had dissolved.

Supersaturation from fine cocrystal 2 is a result of a faster dissolution rate than for larger-sized cocrystal 2 (106–150 and 150–300 μm) mainly because of the larger specific surface area of the smaller particles. Other reasons are differences in the local disorder of the crystal surface and/or the ratio of major to minor crystal surface area. With fine cocrystal 2, the concentration of MA increases before transformation to MA and exhibits supersaturation. In contrast, the dissolution rates for larger-sized cocrystal 2 are slow and no supersaturation was found before the transformation to MA. The solubility (at 4 h) of large-sized cocrystal 2 was lower than that of fine MA. The transformed MA from larger-sized cocrystal 2 maintained their shape and size and might behave the same as larger-sized MA. We concluded

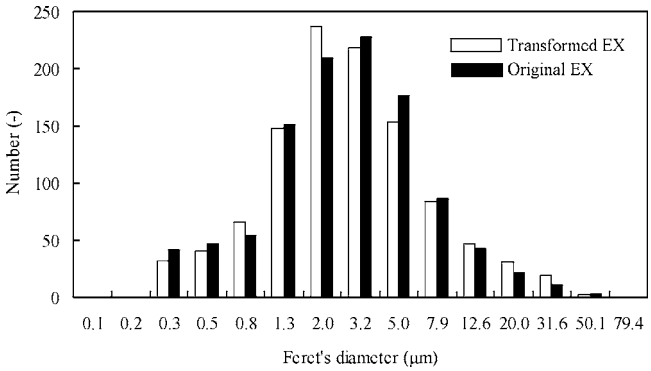

Fig. 10. Particle size distribution of original fine EX and transformed EX from 150–300 μm cocrystal 1 in suspension.

that whether supersaturation from cocrystal 2 occurs or not depends on the competitive success between the dissolution rate and transformation rate. It is also important to control the cocrystalline particle properties (size, crystal surface, *etc*) to improve the solubility potentials of a cocrystal.

The conditions for transformation in these experiments did not include a stirring medium or dispersion of the cocrystal with additives and thus did not mimic the dissolution test conditions. However, the information from the experiments on transformation behavior is valuable for understanding the mechanisms of cocrystal dissolution, which is helpful in estimating *in vivo* absorption and in developing a formulation strategy.

The solid form in aqueous media also influences the solubility. For example, the celecoxib/nicotinamide cocrystal is converted to an amorphous or polymorphic form and the solid form and/or the particle state can be controlled by additives (24). Our results demonstrate that the relationship between transformation rate and dissolution rate is important and that those rates are influenced by solid forms and the state of the particle. In addition, the metastable region of supersaturation of a host compound may also influence the dissolution profile. To determine an effective dissolution profile, a balanced relationship of the solubility of the cocrystal itself and its solid state, the transformation rate, host compound solubility and its solid state, and guest solubility is necessary.

CONCLUSIONS

In this study, we found two novel cocrystals (EX/MAL and MA/SA) from screening using slurry crystallization and characterized the cocrystals using TG-DTA, DSC, PXRD, and single crystal X-ray diffraction. Various sizes of the cocrystals were prepared from solution and dissolution tests were conducted. Dissolution and transformation behavior were examined by PXRD analysis and cocrystal suspensions were observed under polarization microscopy.

Although EX/MAL (cocrystal 1) did not exhibit supersaturation, the dissolution rate of the larger-sized particles (106–150 and 150–300 μm) was improved. The dissolution rates for the larger-sized particles were similar to that of fine EX. The transformation studies demonstrated that all sizes of cocrystal 1 transformed to EX within 1 min, that particle size distribution was similar to fine EX, and that particle size reduction occurred during transformation to EX. The dissolution profile and behavior study of cocrystal 1 suggested that the faster dissolution rate of the larger particles was caused by particle size reduction during transformation.

Although MA/SA (cocrystal 2) of sizes 106–150 and 150–300 μm did not exhibit supersaturation, fine cocrystal 2 did. Intrinsic dissolution rate of cocrystal 2 was higher than that of MA. The transformation behavior studies suggested that MA gradually transformed (2–4 h) and that fine cocrystal 2 was about 2 h slower than of the larger-sized particles. Large-sized MA particles were formed after transformation. The dissolution profile and behavior study of cocrystal 2 suggested that the supersaturation of fine cocrystal 2 was caused by dissolution occurring faster than transformation. Recently, factors influencing the solubility of cocrystals have been reported. In addition to these factors, our study demonstrated that the relationship between the transformation rate and the dissolution rate is also important and that those rates are influenced by the characteristics (size, crystal surface, *etc*.) of the particle. Moreover, it is important to control the cocrystalline particle properties to improve the solubility of a cocrystal.

ACKNOWLEDGEMENTS

The authors acknowledge Syoichi Higo for managerial support and Kyoko Yuyama for assistance with the cocrystal screening experiments.

REFERENCES

1. S. L. Childs, L. J. Chyall, J. T. Dunlap, V. N. Smolenskaya, B. C. Stahly, and G. P. Stahly. Crystal engineering approach to forming cocrystals of amine hydrochlorides with organic acids. Molecular complexes of fluoxetine hydrochloride with benzoic, succinic, and fumaric acids. *J. Am. Chem. Soc.* **126**:13335–13342 (2004), doi:10.1021/ja048114o.
2. S. Basavoju, D. Bostrom, and S. P. Velaga. Indomethacin–saccharin cocrystal: design, synthesis and preliminary pharmaceutical characterization. *Pharm. Res.* **25**:530–540 (2007), doi:10.1007/s11095-007-9394-1.
3. S. L. Morissette, O. Almarsson, M. L. Peterson, J. F. Remenar, M. J. Read, A. V. Lemmo, S. Ellis, M. J. Cima, and C. R. Gardner. High-throughput crystallization: polymorphs, salts, cocrystals and solvates of pharmaceutical solids. *Adv. Drug Deliv. Rev.* **56**:275–300 (2004), doi:10.1016/j.addr.2003.10.020.
4. J. F. Remenar, S. L. Morissette, M. L. Peterson, B. Moulton, J. M. MacPhee, H. R. Guzman, and O. Almarsson. Crystal engineering of novel cocrystals of a triazole drug with 1,4-dicarboxylic acids. *J. Am. Chem. Soc.* **125**:8456–8457 (2003), doi:10.1021/ja035776p.
5. D. P. McNamara, S. L. Childs, J. Giordano, A. Iarriccio, J. Cassidy, M. S. Shet, R. Mannion, E. O'Donnell, and A. Park. Use of a glutaric acid cocrystal to improve oral bioavailability of a low solubility API. *Pharm. Res.* **23**:1888–1897 (2006), doi:10.1007/s11095-006-9032-3.
6. A. V. Trask, W. D. S. Motherwell, and W. Jones. Pharmaceutical cocrystallization: engineering a remedy for caffeine hydration. *Cryst. Growth Des.* **5**:1013–1021 (2005), doi:10.1021/cg0496540.
7. A. V. Trask, W. D. Motherwell, and W. Jones. Physical stability enhancement of theophylline via cocrystallization. *Int. J. Pharm.* **320**:114–123 (2006), doi:10.1016/j.ijpharm.2006.04.018.
8. C. A. Lipinski. Drug-like properties and the causes of poor solubility and poor permeability. *J. Pharmacol. Toxicol. Methods*. **44**:235–149 (2000), doi:10.1016/S1056-8719(00)00107-6.
9. C. A. Lipinski, F. Lombardo, B. W. Dominy, and P. J. Feeney. Experimental and computational approaches to estimate solubility and permeability in drug discovery and development settings. *Adv. Drug Deliv. Rev.* **23**:3–25 (1997), doi:10.1016/S0169-409X(96)00423-1.
10. N. Li, M. D. DeGennaro, W. Liebenberg, L. R. Tiedt, A. S. Zahr, M. V. Pishko, and M. M. de Villiers. Increased dissolution and physical stability of micronized nifedipine particles encapsulated with a biocompatible polymer and surfactants in a wet ball milling process. *Pharmazie*. **61**:595–603 (2006).
11. N., Rasenack, and B. W. Muller. Dissolution rate enhancement by *in situ* micronization of poorly water-soluble drugs. *Pharm. Res.* **19**:1894–1900 (2002), doi:10.1023/A:1021410028371.
12. R. A., Femia, and R. E. Goyette. The science of megestrol acetate delivery: potential to improve outcomes in cachexia. *BioDrugs*. **19**:179–187 (2005), doi:10.2165/00063030-200519030-00004.
13. R. B. Hammond, K. Pencheva, K. J. Roberts, and T. Auffret. Quantifying solubility enhancement due to particle size reduction and crystal habit modification: case study of acetyl salicylic acid. *J. Pharm. Sci.* **96**:1967–1973 (2007), doi:10.1002/jps.20869.

14. E. Merisko-Liversidge, G. G. Liversidge, and E. R. Cooper. Nanosizing: a formulation approach for poorly-water-soluble compounds. *Eur. J. Pharm. Sci.* **18**:113–120 (2003), doi:10.1016/S0928-0987(02)00251-8.
15. R. H., Muller, and C. M. Keck. Challenges and solutions for the delivery of biotech drugs—a review of drug nanocrystal technology and lipid nanoparticles. *J. Biotechnol.* **113**:151–170 (2004), doi:10.1016/j.jbiotec.2004.06.007.
16. R. J. Chokshi, H. Zia, H. K. Sandhu, N. H. Shah, and W. A. Malick. Improving the dissolution rate of poorly water soluble drug by solid dispersion and solid solution: pros and cons. *Drug Deliv.* **14**:33–45 (2007), doi:10.1080/10717540600640278.
17. J. Y. Jung, S. D. Yoo, S. H. Lee, K. H. Kim, D. S. Yoon, and K. H. Lee. Enhanced solubility and dissolution rate of itraconazole by a solid dispersion technique. *Int. J. Pharm.* **187**:209–218 (1999), doi:10.1016/S0378-5173(99)00191-X.
18. G. Ye, S. Wang, P. W. Heng, L. Chen, and C. Wang. Development and optimization of solid dispersion containing pellets of itraconazole prepared by high shear pelletization. *Int. J. Pharm.* **337**:80–87 (2007), doi:10.1016/j.ijpharm.2006.12.028.
19. P. Gao, M. E. Guyton, T. Huang, J. M. Bauer, K. J. Stefanski, and Q. Lu. Enhanced oral bioavailability of a poorly water soluble drug PNU-91325 by supersaturatable formulations. *Drug Dev. Ind. Pharm.* **30**:221–229 (2004), doi:10.1081/DDC-120028718.
20. J. Y. Hong, J. K. Kim, Y. K. Song, J. S. Park, and C. K. Kim. A new self-emulsifying formulation of itraconazole with improved dissolution and oral absorption. *J. Control. Release*. **110**:332–338 (2006), doi:10.1016/j.jconrel.2005.10.002.
21. J. O., Henck and S. R. Byrn. Designing a molecular delivery system within a preclinical timeframe. *Drug Discov. Today.* **12**:189–199 (2007), doi:10.1016/j.drudis.2007.01.006.
22. A. T., Serajuddin, and C. I. Jarowski. Effect of diffusion layer pH and solubility on the dissolution rate of pharmaceutical bases and their hydrochloride salts. I: Phenazopyridine. *J. Pharm. Sci.* **74**:142–147 (1985), doi:10.1002/jps.2600740208.
23. S. L. Childs, G. P. Stahly, and A. Park. The salt-cocrystal continuum: the influence of crystal structure on ionization state. *Mol. Pharm.* **4**:323–338 (2007) doi:10.1021/mp0601345.
24. J. F. Remenar, M. L. Peterson, P. W. Stephens, Z. Zhang, Y. Zimenkov, and M. B. Hickey. Celecoxib:nicotinamide dissociation: using excipients to capture the cocrystal's potential. *Mol. Pharm.* **4**:386–400 (2007), doi:10.1021/mp0700108.
25. T. A. Traina, I. Poggesi, M. Robson, A. Asnis, B. A. Duncan, A. Heerdt, C. Dang, D. Lake, M. Moasser, K. Panageas, P. Borgen, L. Norton, C. Hudis, and M. N. Dickler. Pharmacokinetics and tolerability of exemestane in combination with raloxifene in postmenopausal women with a history of breast cancer, *Breast Cancer Res. Treat.* (20 October 2007), doi:10.1007/S10549-007-9787-1.
26. S. S., Yeh, and M. W. Schuster. Megestrol acetate in cachexia and anorexia. *Int. J. Nanomedicine*. **1**:411–416 (2006), doi:10.2147/nano.2006.1.4.411.
27. A. Farinha, A. Bica, and P. Tavares. Improved bioavailability of a micronized megestrol acetate tablet formulation in humans. *Drug Dev. Ind. Pharm.* **26**:567–570 (2000), doi:10.1081/DDC-100101270.
28. Adis International Limited. Megestrol acetate NCD oral suspension. Par Pharmaceutical: megestrol acetate nanocrystal dispersion oral suspension, PAR 100.2, PAR-100.2. *Drugs R. D.* **8**:251–254 (2007), doi:10.2165/00126839-200708040-00005.
29. G. G. Zhang, R. F. Henry, T. B. Borchardt, and X. Lou. Efficient co-crystal screening using solution-mediated phase transformation. *J. Pharm. Sci.* **96**:990–995 (2007), doi:10.1002/jps.20949.
30. N. Takata, K. Shiraki, R. Takano, Y. Hayashi, and K. Terada. Cocrystal screening of stanolone and mestanolone using slurry crystallization. *Cryst. Growth Des.* (2008), doi:10.1021/cq800156k.
31. A. Altomare, G. Cascarano, C. Giacovazzo, A. Guagliardi, M. C. Burla, G. Polidori, and M. Camalli. SIR92—a program for automatic solution of crystal structures by direct methods. *J. Appl. Cryst.* **27**:435–436 (1994), doi:10.1107/S002188989400021X.
32. R. Takano, K. Sugano, A. Higashida, Y. Hayashi, M. Machida, Y. Aso, and S. Yamashita. Oral absorption of poorly water-soluble drugs: computer simulation of fraction absorbed in humans from a miniscale dissolution test. *Pharm. Res.* **23**:1144–1156 (2006), doi:10.1007/s11095-006-0162-4.
33. S. J. Nehm, B. Rodriguez-Spong, and N. Rodriguez-Hornedo. Phase solubility diagrams of cocrystals are explained by solubility product and solution complexation. *Cryst. Growth Des.* **6**:592–600 (2006), doi:10.1021/cg0503346.
34. H. L. Vos. Thermal stability of some WHO melting point reference compounds. *Pharm. Weekbl.* **104**:619–629 (1969).
35. S. Budavari, M. J. O'Neil, A. Smith, and P. E. Hekelman. *The Merck Index*. 13Merck & CO, New Jersey, 1989.
36. Y. Suzuki, K. Muraishi, and K. Matsuki. Thermal behavior of dicarboxylic acids. Determination of melting points by DTA. *Thermochim. Acta*. **211**:171–180 (1992), doi:10.1016/0040-6031(92)87017-5.
37. K., Muraishi, and Y. Suzuki. The thermal behavior of dicarboxylic acids in various atmospheres. *Thermochim. Acta*. **232**:195–203 (1994), doi:10.1016/0040-6031(94)80059-6.
38. K. Seefeldt, J. Miller, F. Alvarez-Nunez, and N. Rodriguez-Hornedo. Crystallization pathways and kinetics of carbamazepine–nicotinamide cocrystals from the amorphous state by *in situ* thermomicroscopy, spectroscopy, and calorimetry studies. *J. Pharm. Sci.* **96**:1147–1158 (2007), doi:10.1002/jps.20945.
39. M. Tenho, P. Heinanen, V. P. Tanninen, and V. P. Lehto. Does the preferred orientation of crystallites in tablets affect the intrinsic dissolution. *J. Pharm. Biomed. Anal.* **43**:1315–1323 (2007), doi:10.1016/j.jpba.2006.10.038.
40. A., Noyes, and W. Whitney. The rate of solution of solid substances in their own solution. *J. Am. Chem. Soc.* **19**:930–940 (1897), doi:10.1021/ja02086a003.
41. G. Y. Kwei, L. B. Novak, L. A. Hettrick, E. R. Reiss, D. Ostovic, A. E. Loper, C. Y. Lui, R. J. Higgins, I. W. Chen, and J. H. Lin. Regiospecific intestinal absorption of the HIV protease inhibitor L-735,524 in beagle dogs. *Pharm. Res.* **12**:884–888 (1995), doi:10.1023/A:1016269206048.
42. N. Rodriguez-Hornedo, S. J. Nehm, K. F. Seefeldt, Y. Pagan-Torres, and C. J. Falkiewicz. Reaction crystallization of pharmaceutical molecular complexes. *Mol. Pharm.* **3**:362–367 (2006), doi:10.1021/mp050099m.
43. S. Yalkowsky, and Y. He. *Handbook of Aqueous Solubility Data*. CRC, Routledge, 2003.